

HYDRODYNAMIC FORCES ON MARINE CABLES WITH PET SHROUDS

Min-Chih Huang*

*Department of Naval Architecture & Marine Engineering
National Cheng Kung University, Tainan, Taiwan, R. O. C.

Shyang-Yu Baur**

**Department of Hydraulic & Ocean Engineering
National Cheng Kung University, Tainan, Taiwan, R. O. C.

Keywords: Vortex-Shedding, Cable Strumming, PET Shrouds, Suppression Device

ABSTRACT

The hydrodynamic forces on a bare nylon cable with a diameter of 2.1cm in steady uniform flows are determined experimentally. The range of flow velocity is from 0.37 to 1.35m/s, which corresponds to Reynolds number in the range of $0.95-3.5 \times 10^4$. The hydrodynamic forces on the same cable with perforated and with non-perforated shrouds, made from 1.25-liter PET bottles, are also determined in the same velocity range.

This paper presents tested results for three different models: bare cable, cable with 50% area perforated shrouds and cable with non-perforated shrouds in the reduced velocity range of 5.63-10.66, 11.20-20.72, 11.37-21.83, respectively. Both in-line and transverse force coefficients are given as functions of the reduced velocity. The applications of PET shrouds as fish/kelp aggregation device and as strumming suppression device for marine cables are discussed.

串通保特瓶覆蓋物纜繩之流體力

黃明志*

*國立成功大學造船及船舶機械工程系

薄祥裕**

**國立成功大學水利及海洋工程所

關鍵詞：渦流脫落，纜繩共振，保特瓶覆蓋物，並振壓制器

摘要

本文利用試驗決定一直徑2.1公分之光滑尼龍纜繩在穩態均勻流中之流體力。試驗時流速範圍介於0.37至1.35m/s之間，其所對應之雷諾數範圍為 $0.95-3.5 \times 10^4$ 。同一纜繩串通1.25公升之保特瓶覆蓋物亦在相同之流速範圍中試驗求得其流體力，至於覆蓋物模型則採用光滑之保特瓶或開孔之保特瓶。

本文提供以下三種不同模型之試驗結果：光滑纜繩，纜繩外串百分之五十開孔面積之保特瓶，與纜繩外串光滑之保特瓶。此三種模型試驗之相對流速範圍各介於5.63—10.66, 11.20—20.72, 11.37—21.83之間。文中探討正向流阻力係數，側向振動力係數與相對流速變化關係之試驗結果。文中亦討論採用保特瓶覆蓋物為人工浮漁礁，海藻聚集物，與纜繩共振壓制器之應用性。

INTRODUCTION

Synthetic marine cables are often used to support buoys, instrument arrays and platforms. They are highly flexible, nonlinear structures. The adaptive nature of cables often makes them vulnerable to the hydrodynamic forces induced by vortex shedding in a cross-flow. These alternating forces can cause large amplitude oscillations of the cable system when the forces occur at or near one of its natural frequencies. The induced cable oscillations in turn control the vortex shedding so that it is frequency synchronized to the motion. This phenomenon, called cable strumming, often results in larger hydrodynamic forces, increased fatigue and structural failures.

The vortex induced cable oscillations may be studied experimentally by forced vibration or by self excitation of the test cable, since the similarities in the wake structures from these two experiments were previously validated by Griffin [4]. Recent studies include those of Peltzer [7], Peltzer and Rooney [8], Griffin and Vandiver [5], Vandiver and Chung [9]. The test cables in these studies are all composite type, with a rubber hose or a polyurethane jacket wrapped around several braided Kevlar ropes.

The authors recently conducted a series of laboratory tests on moored nylon cable arrays with PET shrouds, which were designed as fish and kelp aggregation devices in coastal waters. These shrouds were made from commercial 1.25-liter PET bottles with punched bottom holes through which a cable was passed loosely, and the whole fish aggregation device can be constructed easily in situ from a small fishing boat.

Measured hydrodynamic forces and vibration frequencies of strumming cables in steady uniform flows are presented for three different models: bare cable, cable with 50% area perforated shrouds and cable with non-perforated shrouds. The experimental results are from flow-induced self-vibration experiments conducted in a circulation water tunnel.

Measured vibration characteristics indicate

that perforated shrouds made from commercial PET bottles may also be considered as strumming suppression device for synthetic marine cables.

EXPERIMENTAL SETUP

1. Test Rig

The experiments were conducted at a horizontal circulation tunnel which has a open-water test section 3.8m long, 1.2m wide and 0.825m deep. Uniform steady flow with speed up to 1.35 m/s can be generated in the test section.

In the middle of the test section, a steel frame was placed on the sides of the tunnel to support a circular rod which can be moved in the vertical direction. A two-component force transducer of the type Nissho LMC-3504-5 with a maximum load capacity of 5kg was fixed to the end of rod. Another force transducer of the type Kyowa Model LUB-50KB with a maximum axial load capacity of 50kg was fixed on the bottom. A test cable was then simply connected to the top force transducer via an universal joint, and to the bottom force transducer via a swivel. The cable tension was then adjusted at the top through a turnbuckle on the movable rod. This test arrangement is shown in Fig. 1, where a 16cm long cable was kept above the free surface during the experiments.

2. Velocity Measurements

One meter upstream of the test model, a simple mechanism was constructed to lower a current meter to any vertical position in the test section. The current meter was a Marsh-McBirney Model 523, dual-axis, electromagnetic type. The sensor outputs were passed through low pass filters. A time constant of 5 seconds, with a 3dB corner frequency of 0.0306 Hz, was set during the tests. The magnitude of uniform current was measured 0.1m below the free surface during the tests.

3. Test Models

Three models were tested during the experiments: bare cable, cable with perforated PET shrouds, and cable with non-perforated PET shrouds. The cable used in the tests was a length of nylon synthetic fiber ropes with a nominal diameter of $D=2.1\text{cm}$. The shrouds were made from two 1.25-liter PET bottles and has a maximum diameter of 8.65cm. A circular hole was punched at the bottom of each bottle through which a cable was passed loosely. The perforated shrouds have several circular holes with 5cm diameter, and has a 50 percent open area. These test models are illustrated in Fig. 2.

4. Data Acquisition

The inline and transverse forces on the test model was calculated from the top force transducer measurements, taken account of the non-submerged part of cable; while the axial force was measured by the bottom force transducer. The analog signals from the force transducers were amplified and passed through a 100 Hz low pass filter, digital force measurements were then obtained from an A/D converter, at a sampling rate of 50 Hz with a 12 s sampling duration, and stored for data analysis. A standard fast Fourier transform method were used to calculate the axial, inline and transverse force spectrums from 0 to 25 Hz with the frequency resolution of 0.0977Hz.

EXPERIMENTAL RESULTS

1. Free Vibration Tests

Free vibration tests were first conducted to find the natural frequencies of test models in the range of cable tension from 10 to 20kg. These experimental results are illustrated in Fig. 3 where the variation of natural frequencies with the tensions are shown to be well represented by linear regression lines. The natural frequency of bare cable is approximately 2.2-2.7 times that of cable with shrouds under the same tension.

2. Test Procedure

The tests reported herein constitute three sequences corresponding to three different models. Each test sequence comprises typically 20 to 25 different flow speeds. During each test sequence the cable was first pretensioned at 10kg and the magnitude of uniform current was adjusted to the lowest speed of the test tunnel (0.25m/s). After the force and velocity measurements were taken for this flow speed, the magnitude of uniform current was increased to a higher speed without readjusting the cable tension. The whole data acquisition sequence continued in this fashion until the flow speed reached 1.5 m/s. Those tests with flow speed over 1.35 m/s were not analysed in this study since the flow was too turbulent.

The mean cable tension under each flow speed was found from the axial force spectrum. The mean tension lies in the range of 12-20kg, 13-22kg, and 13-27kg, respectively, for the three test sequences. The corresponding natural frequency for each test was then calculated from the linear regression and extrapolation lines shown in Fig. 3.

3. Test Range

The velocity range of the tests reported herein was $U=0.37\text{—}1.35\text{ m/s}$, Where U =the magnitude of the uniform flow. The corresponding Reynolds number of the bare cable tests was $Re=0.95\text{--}3.50 \times 10^4$, in which Re is defined by

$$Re = \frac{U D}{\nu} \quad (1)$$

where ν =the kinematic viscosity. The hydrodynamic forces on the same cable with perforated and with non-perforated PET shrouds were also determined in the same velocity range.

This paper presents tested results in the range of reduced velocity of 5.63—10.66, 11.20—20.72,

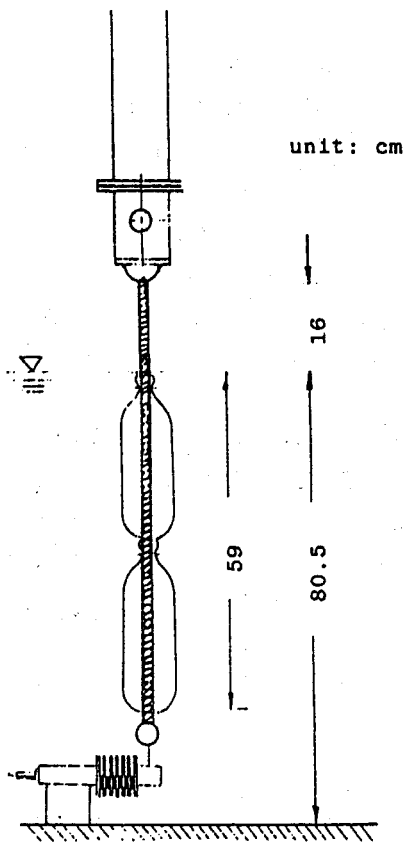


Fig. 1. Experimental setup

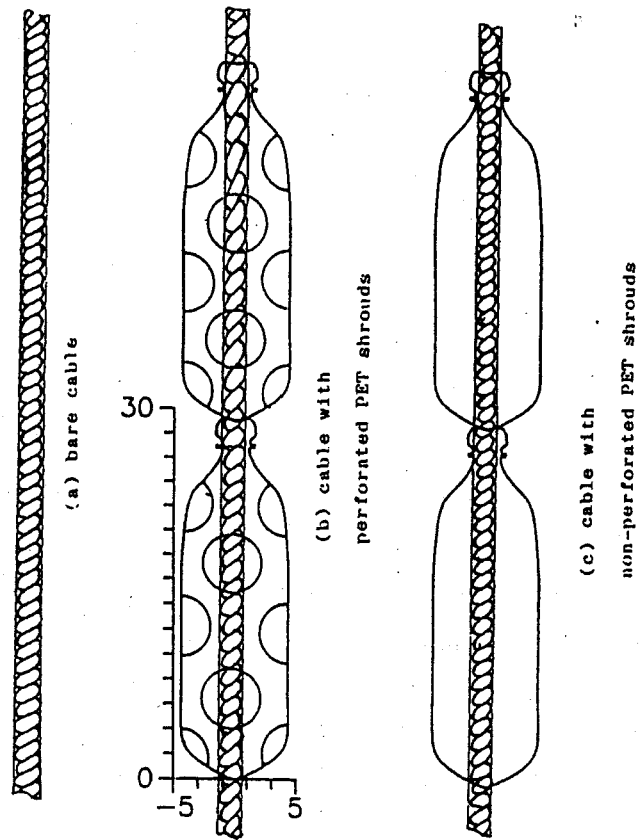


Fig. 2. Test models

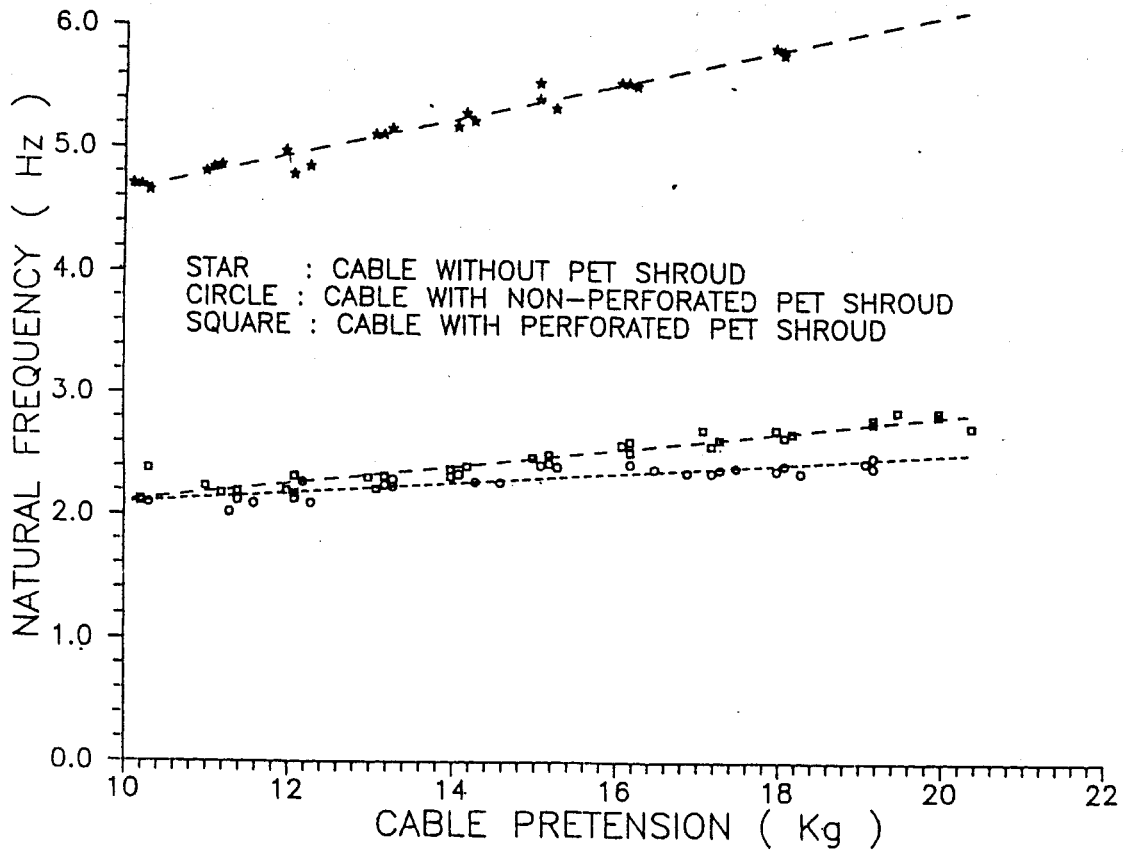


Fig. 3. Variation of natural frequency with cable tension

11.37—21.83, for three different models: bare cable, cable with 50% area perforated shrouds and cable with non-perforated shrouds, respectively. The reduced velocity, V_r , is defined by

$$V_r = \frac{U}{D f_n} \quad (2)$$

Where f_n = the natural frequency of the vibrating model. A value of cable diameter $D=2.1\text{cm}$ is used for all three test models.

4. Transverse Force Spectrums

All the transverse force spectrums for the bare cable model in the whole test range are narrowbanded, each with a single peak fundamental frequency, f_0 , which is identified as the (synchronized or nonsynchronized) vortex shedding frequency. The vortex shedding frequency lies in the range of $4.9 < f_0 < 6.1$ in the reduced velocity range of $5.63 < V_r < 10.66$.

Examples of the transverse force spectrums for the bare cable at various speeds are illustrated in Figs. 4. This figure contains six spectrums where the vortex shedding frequency is shown to increase with increasing reduced velocity. Fig. 4 also indicates that the excitation range for the transverse cable oscillations (strumming) are likely to start at $V_r > 5.6$. As a comparison, the excitation range of the transverse oscillations for a circular cylinder in water was previously identified by Every et al. [1] to extend over $4.5 < V_r < 10$, with maximum amplitude falling within the range of $6.5 < V_r < 8$.

Examples of the transverse force spectrums for cable with perforated shrouds at various speeds are shown in Fig. 5. The peak frequency of each spectrum decreases significantly when compared with that of a bare cable under the same flow speed and tension. The vortex shedding frequency lies in the range of $1.86 < f_0 < 3.03$ in the reduced velocity range of $11.20 < V_r < 20.72$. Higher frequency components in the force spectrums are also shown in Fig. 5, which

are induced by the incomplete vortex shedding from the perforated shrouds.

Examples of the transverse force spectrums for cable with non-perforated shrouds are shown in Fig. 6. The vortex shedding frequency lies in the range of $1.09 < f_0 < 2.57$ in the reduced velocity range of $11.37 < V_r < 21.83$. The peak frequency of the force spectrum is smaller than that of cable with perforated shrouds under the same flow speed and tension. The magnitudes of higher harmonics, especially the third harmonics, are also increased. These higher frequency oscillations are mostly induced by the longitudinal vortex associated with the non-uniform cross section of the PET bottles.

5. Strouhal Numbers

The vortex shedding frequency, f_0 , identified from the transverse force spectrum, is used to calculate the Strouhal number, St , which is defined as

$$St = \frac{f_0 D}{U} \quad (3)$$

The variations of Strouhal number, St , with reduced velocity for the three test models are shown in Fig. 7, where a value of cable diameter $D=2.1\text{cm}$ is used for all three models. Zdravkovich [11] indicated that the almost constant frequency of vortex shedding within the range of synchronization leads to a continuously decrease of the Strouhal number. Fig. 7 illustrated this phenomenon in the range of $5.6 < V_r < 8.2$ for a bare cable where the Strouhal number decreased from 0.178 to 0.159, and in the whole range of the reduced velocity for cable with perforated shrouds. Fig. 7 also shows that an almost constant Strouhal number (lies in the range of 0.0433—0.0398) is found for cable with non-perforated shrouds, which indicates that the test (velocity) range is not large enough to identify the whole synchronization range of this model.

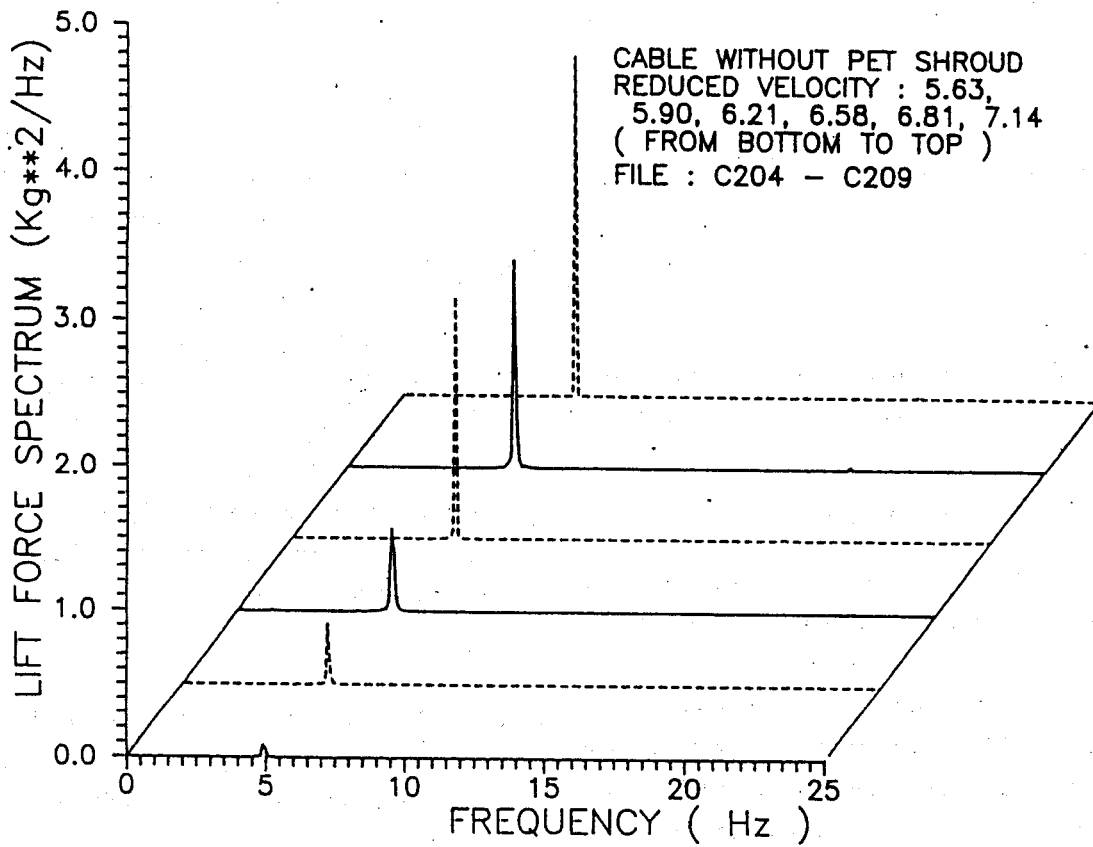


Fig. 4. Transverse force spectrums for a bare nylon cable

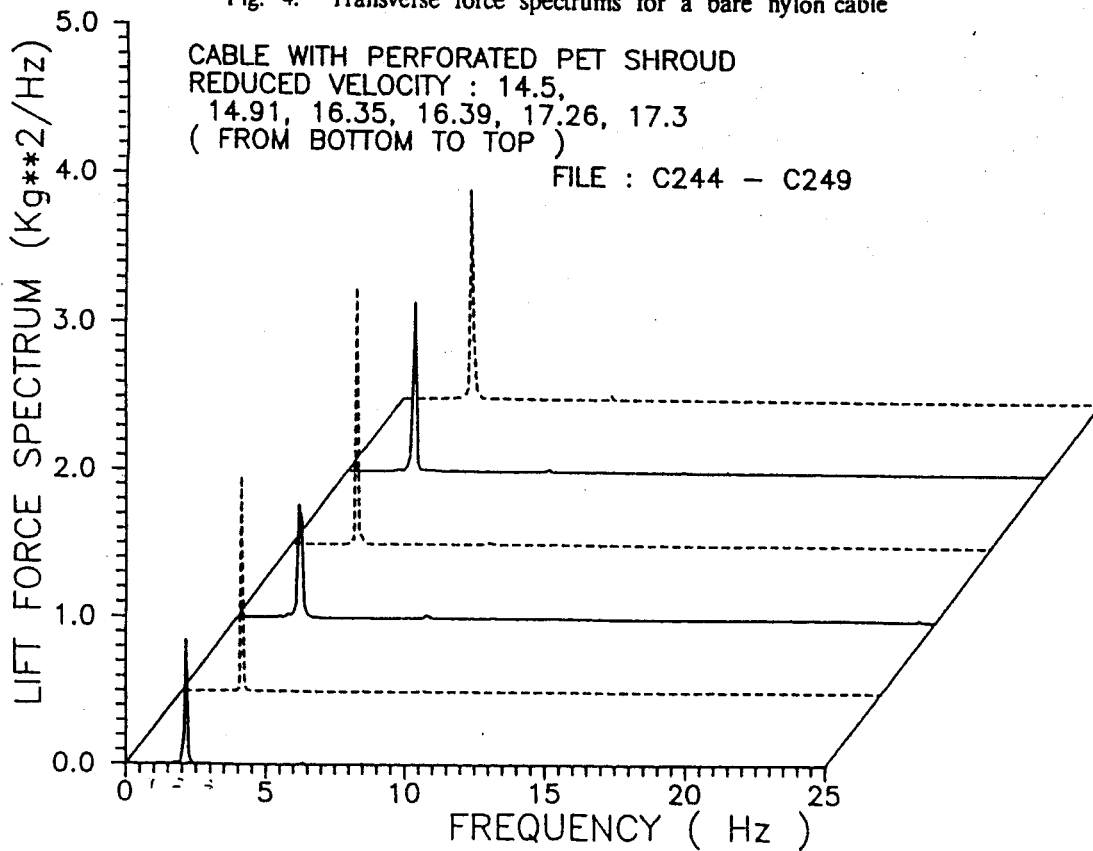


Fig. 5. Transverse force spectrums for a cable
with perforated PET shrouds

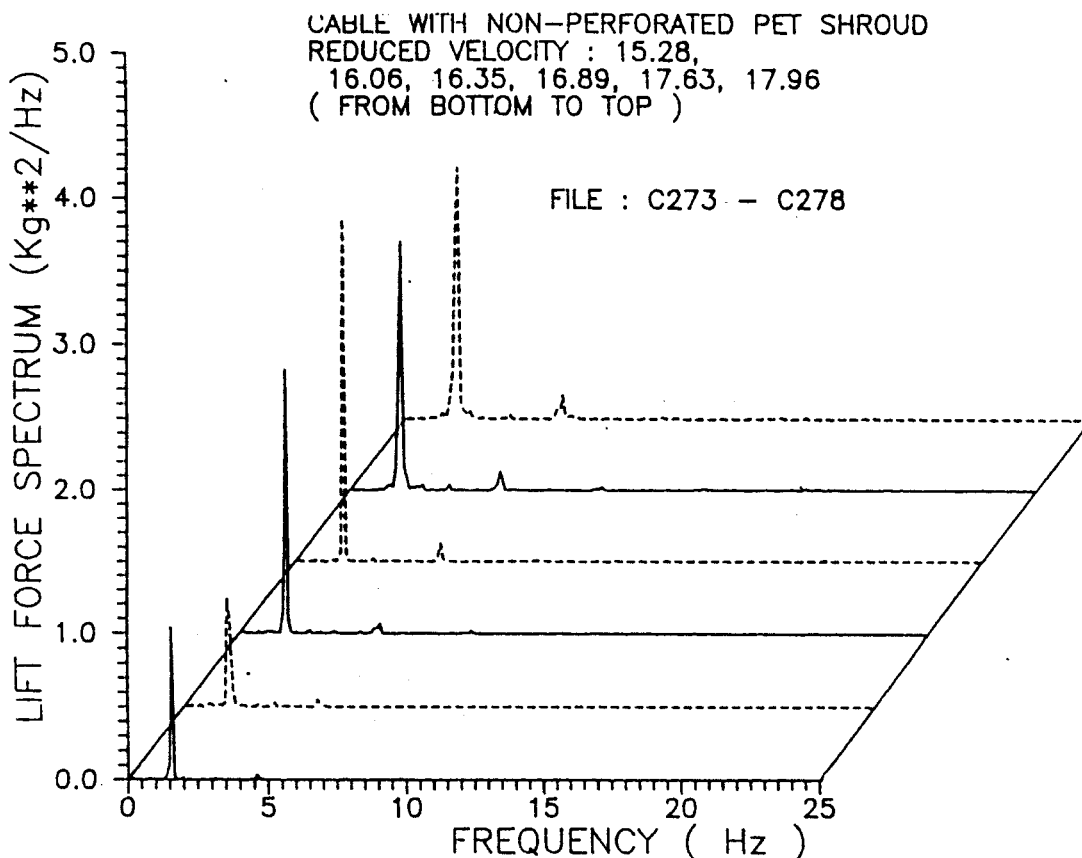


Fig. 6. Transverse force spectrums for a cable with non-perforated PET shrouds

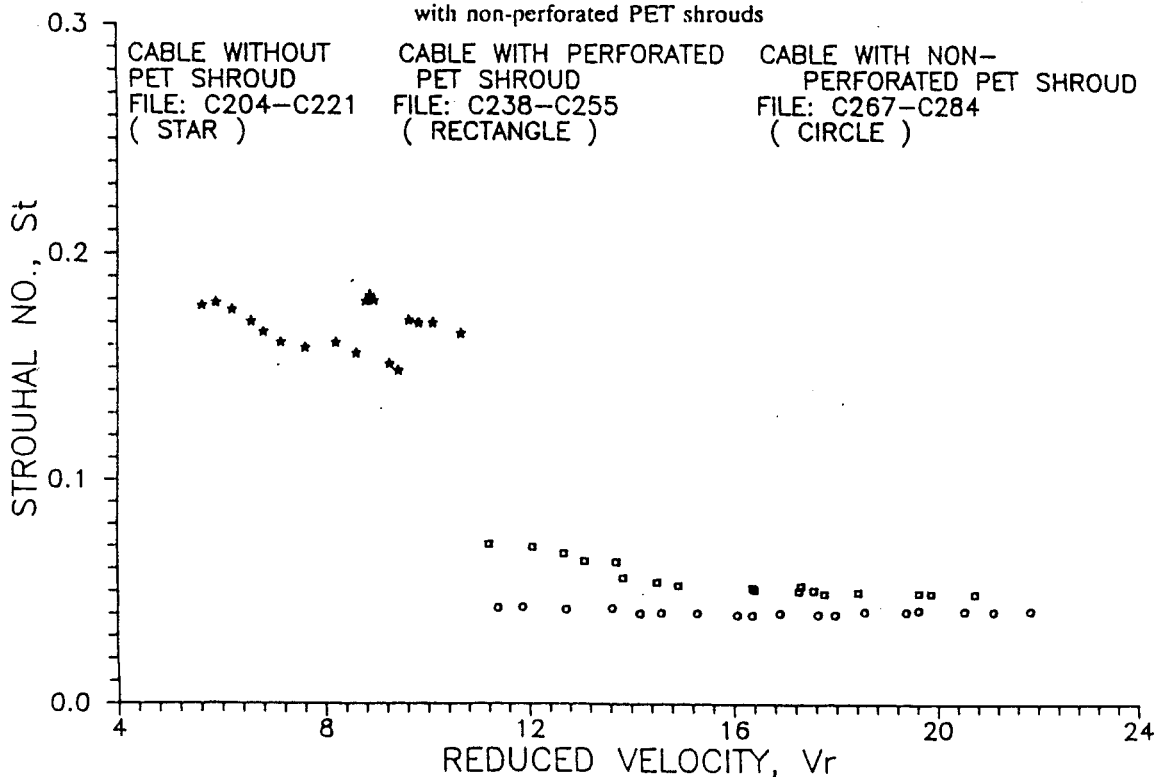


Fig. 7. Variation of Strouhal number with reduced velocity

Another aspects revealed in Fig. 7 is that the Strouhal numbers (or, vortex-shedding frequencies) for cable and for cable with non-perforated shrouds follow approximately the inverse diameter law, at a ratio of 8.65 to 2.1. The variation of Strouhal number for cable with perforated shrouds then lies in between these two extremes.

6. Force Coefficients

The measured force traces resemble those of harmonic signals which may be approximated in terms of finite Fourier series. For example, the transverse lift force may be expressed as

$$F_L(t) = \frac{1}{2} \rho D U^2 [C_L(0) + \sum_{n=1}^N C_L(n) \cos(2n \pi f_o t + \epsilon_n)] \quad (4)$$

in which t =time, $F_L(t)$ =lift force variation, ρ =the fluid density, $C_L(0)$ =the mean lift force coefficient, $C_L(n)$ =the fundamental and higher harmonic lift force coefficients, ϵ_n =the phase, and N =number of components. The in-line drag may be expressed in a similar form.

The transverse lift force coefficients, $C_L(\)$ s, for a bare cable are presented in Fig. 8, while the in-line drag force coefficients, $C_D(\)$ s, are presented in Fig. 9. The mean forces measurements were directly nondimensionalized to obtain the mean lift and drag coefficients, $C_L(0)$ and $C_D(0)$. However the fundamental lift and drag coefficients, $C_L(1)$ and $C_D(1)$, were calculated from the sums of force spectral contents in an interval of 20 frequency increments centered at of [3]. The force coefficients for the higher harmonic force components, e. g., $C_L(2)$ and $C_D(2)$, were calculated similarly.

Figs. 8-9 indicate that:

1. In general the vortex shedding results in alternating lift forces at the fundamental frequency, while the inline drags alternated at the second harmonic.

2. Synchronization for both transverse and in-line cable oscillations lies in the range of $5.6 < V_r < 8.2$. Data shown in these two figures support what has been described previously in Figs. 4 and 7. The maximum amplitudes of force coefficients $C_L(1)$ and $C_D(2)$ occurs near $V_r=6.6$, with $C_L(1)=3.9$ and $C_D(2)=1.33$.
3. Transverse oscillations occur within three adjacent regions. The first is in the range of $5.6 < V_r < 8.2$. The second region lies in the range of $8.6 < V_r < 9.2$, with maximum amplitude occurs near $V_r=8.9$. The third region extends behind $V_r=9.5$.

The lift and drag force coefficients for cable with perforated shrouds are shown in Figs. 10 and 11, respectively. A value of cable diameter $D=2.1$ cm was also used henceforth to calculate the force coefficients of cable with shrouds. Figs. 10-11 indicate that:

1. The transverse forces and inline drags are also alternating at the vortex shedding frequency and their second harmonic, respectively.
2. Both transverse and in-line strumming starts at $V_r > 13.8$ and lies in the range of $13.8 < V_r < 20.7$. The maximum amplitudes of force coefficients $C_L(1)$ and $C_D(2)$ occur near $V_r=14.9$ and 16.4 , respectively, with $C_L(1)=2.6$ and $C_D(2)=1.76$.
3. Prior to and after the onset of synchronization ($V_r=13.8$), the mean drag coefficient $C_D(0)$ can be approximated by two constant values of 2.85 and 3.8 in the ranges of $11 < V_r < 13.7$ and $13.85 < V_r < 17.3$, respectively.
4. The in-line strumming in the range of $14.9 < V_r < 17.3$ can be characterized by an almost constant drag coefficient of $C_D(2)=1.7$.

The lift and drag force coefficients for cable with non-perforated shrouds are shown in Figs. 12 and 13, respectively. The results indicate that:

1. The dominant frequencies of the lift forces and inline drags are still the vortex shedding frequencies and their second harmonics. However the magnitude of the third harmonic lift force coefficient, $C_L(3)$, increased rapidly as V_r increases.

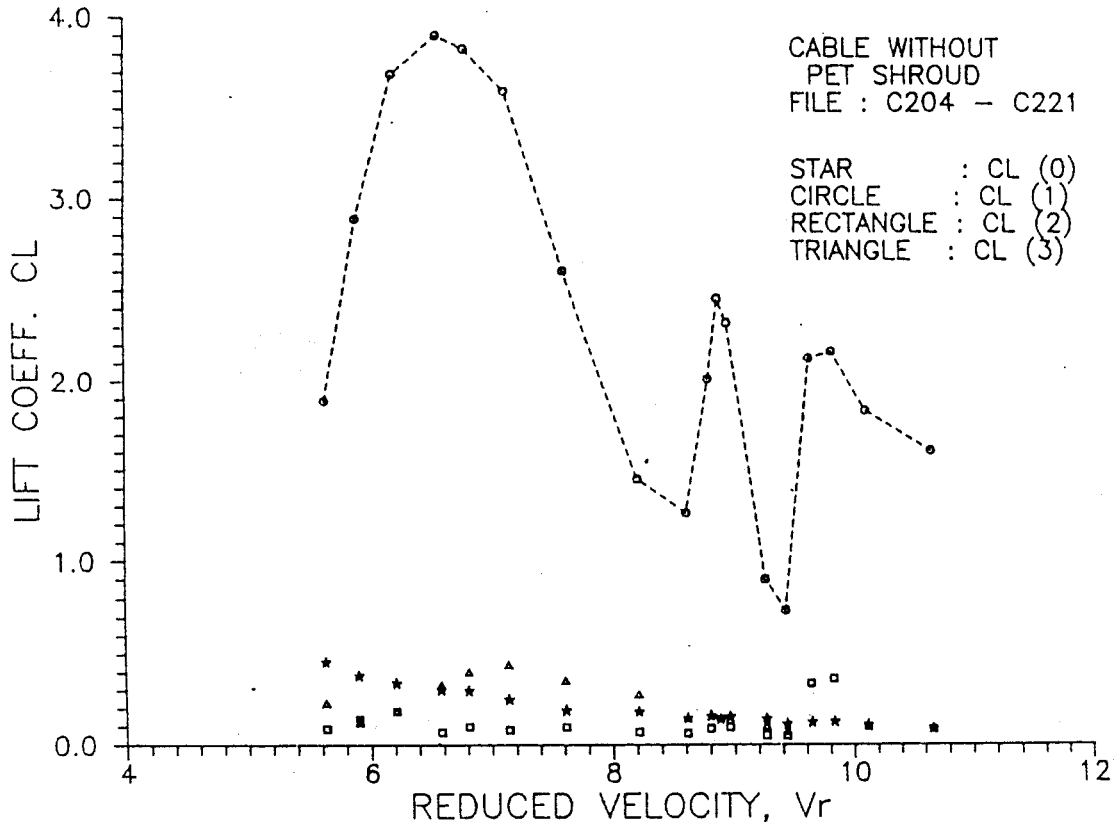


Fig. 8. Transverse lift force coefficients for a bare nylon cable

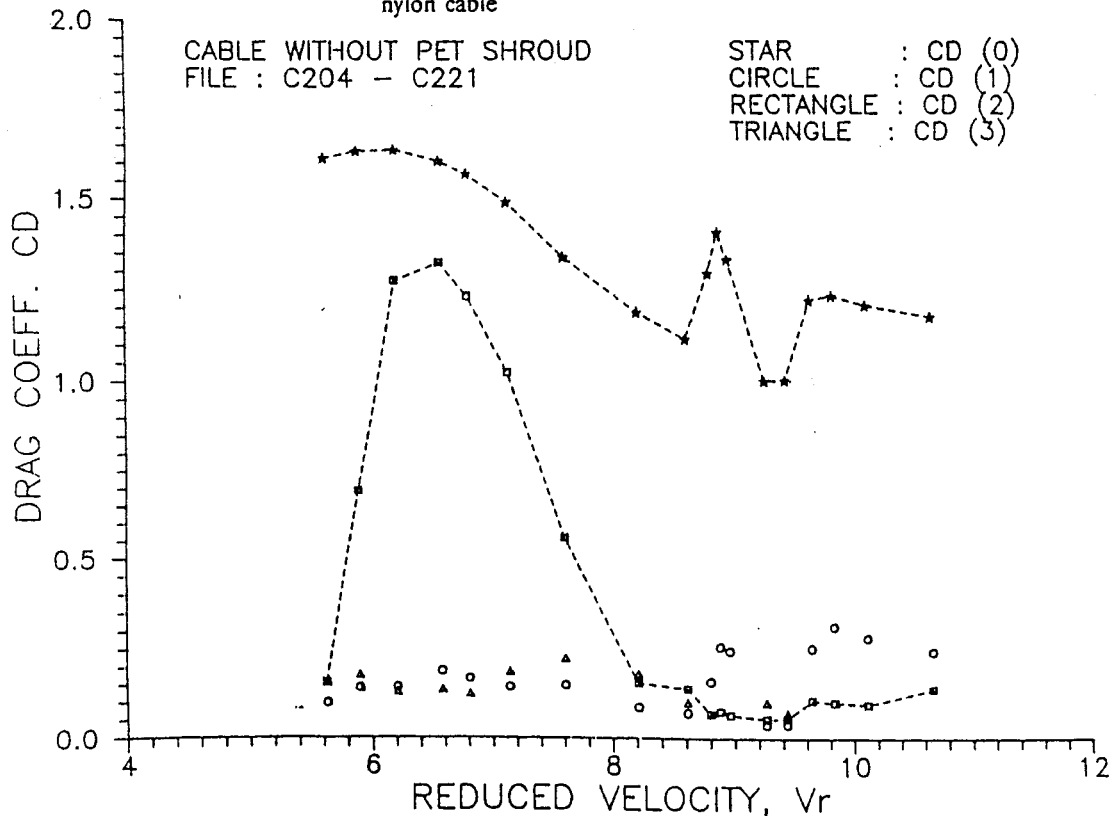


Fig. 9. Inline drag force coefficients for a bare nylon cable

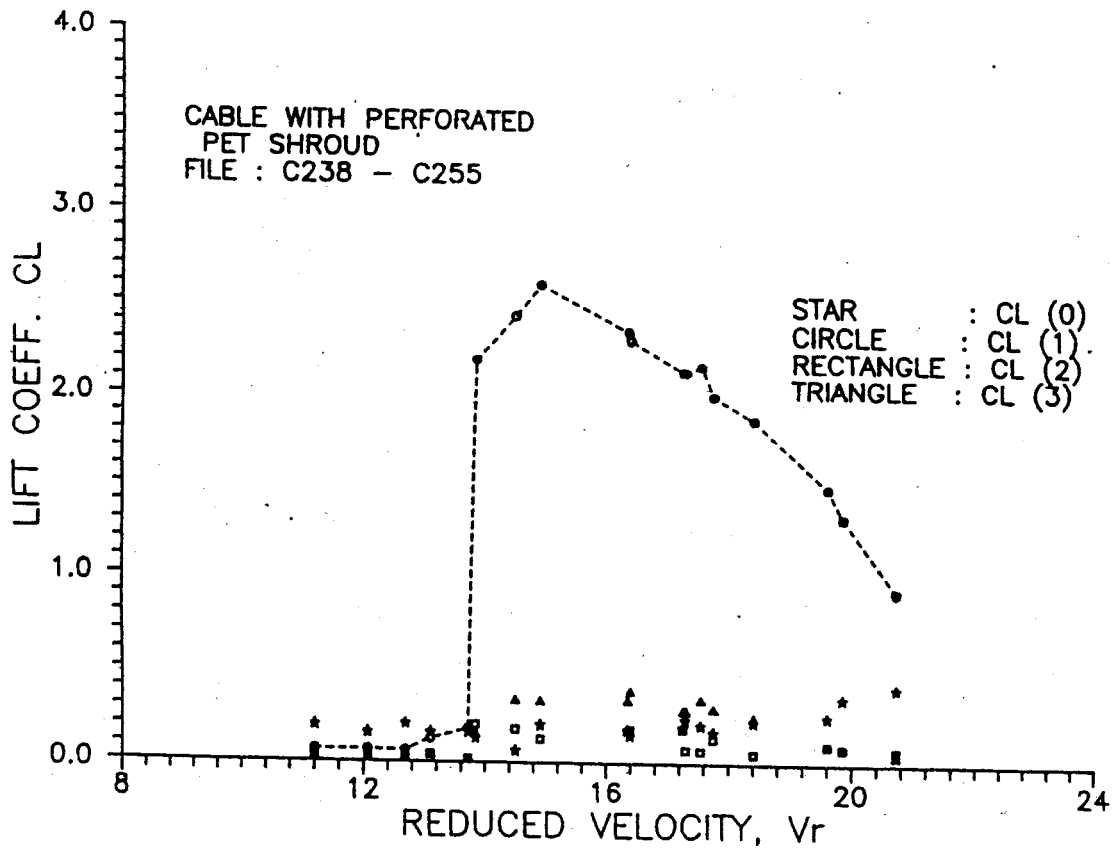


Fig. 10. Transverse lift force coefficients for a cable with perforated PET shrouds

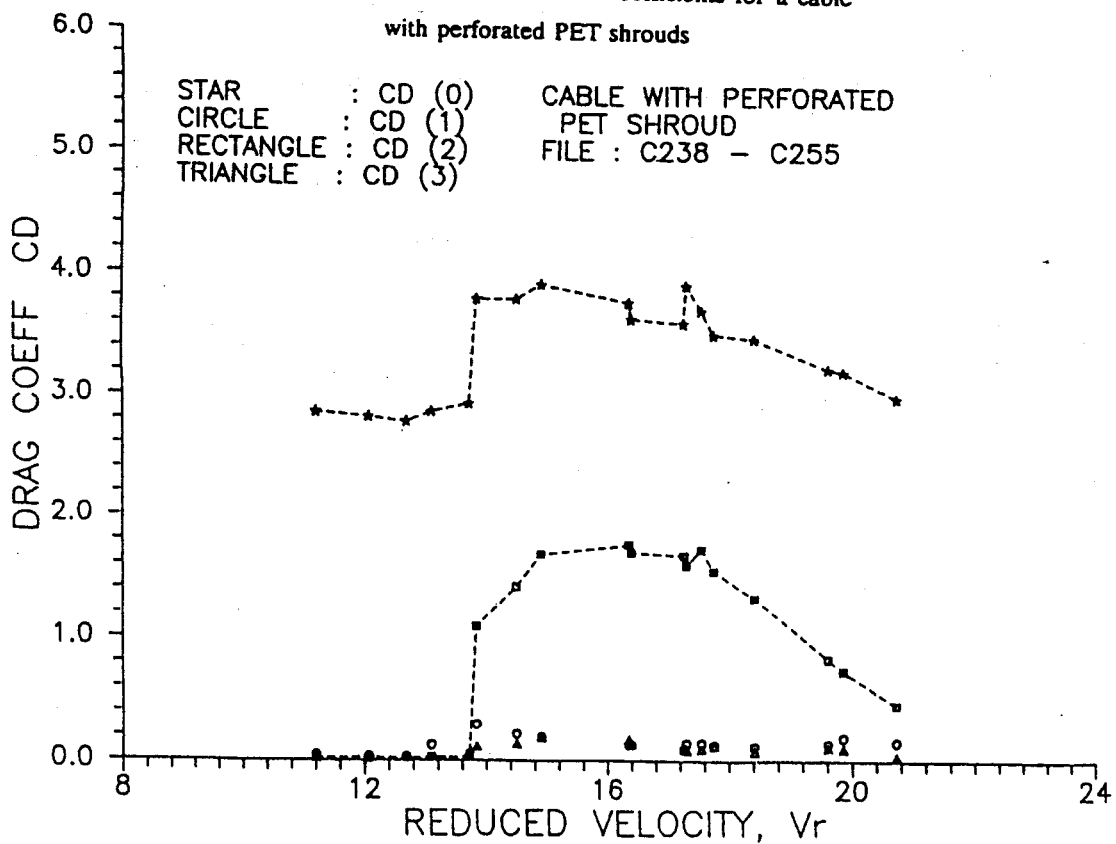


Fig. 11. Inline drag force coefficients for a cable with perforated PET shrouds

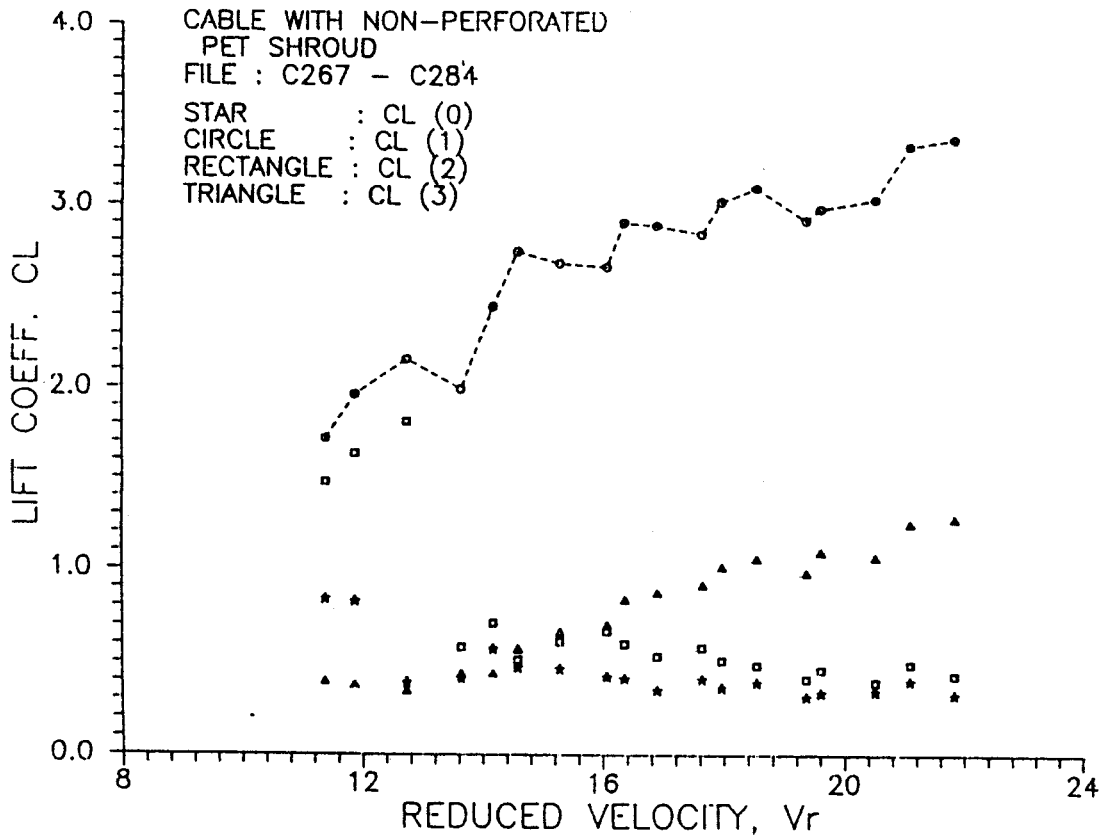


Fig. 12. Transverse lift force coefficients for a cable

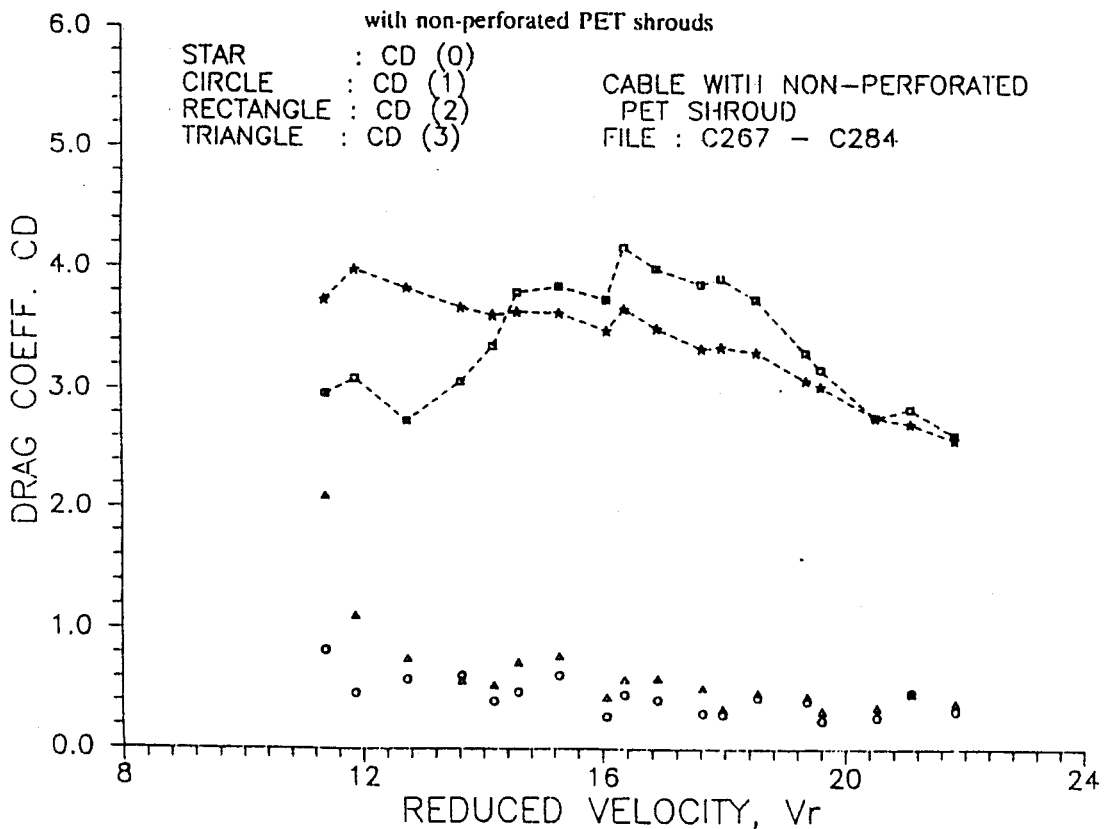


Fig. 13. Inline drag force coefficients for a cable

with non-perforated PET shrouds

This phenomenon was illustrated previously in the transverse force spectrums.

2. The fundamental lift coefficient, $C_L(1)$, increases almost linearly with increasing V_r in the range of $11.37 < V_r < 21.83$, also indicating that the test range is not large enough to cover the whole synchronization range for this model. The maximum amplitude of force coefficients $C_L(1)$ occurs at the end of test range with $C_L(1) = 3.37$ at $V_r = 21.83$.
3. The mean and the second harmonic drag coefficients, $C_D(0)$ and $C_D(2)$, are approximately of the same magnitudes for the whole range of $11.37 < V_r < 21.83$. The maximum force coefficient $C_D(2)$ occurs near $V_r = 16.4$ with a value of 4.16.
4. Comparison of Fig. 11 and Fig. 13 indicates that the mean drag on a cable with non-perforated shrouds is approximately the same as that on a cable with 50% area perforated shrouds. However the amplitude of the second harmonic drag coefficient on a cable with non-perforated shrouds is at least twice as large as that of cable with perforated shrouds.

APPLICATIONS

Marine cables made of synthetic fiber ropes are mostly constructed by twisting several strands around each other helically. This helical shape introduces disturbances on the surface which further interact with the vortex shedding mechanism, and the wake structure becomes more complicated when compared with that behind a cylinder. Since the alternation of structural stiffness or damping of a cable system is often not practical, cable strumming is best avoided or reduced by attaching some form of flow spoiling devices to disrupt the vortex shedding process. The helical shape and the flexible nature of cable itself present mechanical difficulties of attaching any fixed type flow spoiling device, even when the cable is wrapped with a smooth tubing. Numerous strumming suppression devices have been pro-

posed and tested in the past, such as those reviewed by Hafen et al., [6], Fabula and Bedore [2], Zdravkovich [10], and Every et al., [1].

Measured vibration characteristics in this study indicate that perforated shrouds made from commercial PET bottles may be considered as strumming suppression device for synthetic marine cables. Synchronization ranges for both transverse and in-line oscillations are $5.6 < V_r < 8.2$ and $13.8 < V_r < 20.7$, for bare cable and cable with perforated shrouds, respectively. Since the natural frequency of bare cable is approximately 2.2-2.7 times that of a cable with shrouds in the same range of mean tension, therefore, the two reduced velocity ranges correspond to approximately the same flow velocity range where synchronization occurs. The maximum force coefficients $C_L(1)$ and $C_D(2)$ for a strumming bare cable are $C_L(1) = 3.9$ and $C_D(2) = 1.33$, while the corresponding amplitudes are $C_L(1) = 2.6$ and $C_D(2) = 1.76$ for a cable with 50% area perforated shrouds.

The advantages of using perforated shrouds made from commercial PET bottles as strumming suppression devices for marine cables are:

1. Discarded PET bottles are easily obtained and the shrouds can be fabricated at very low cost.
2. PET shrouds are omnidirectional and each shroud (i.e., each bottle) acts as a module. Stoppers can be clamped to any two points on the cable to contain a desired length of shrouds. The shrouds will not present fixing and handling problems.
3. They are easy to be replaced when damaged.

The disadvantage of perforated PET shrouds is similar to that of any strumming suppression device, i.e., they tend to increase the in-line drag. As a comparison, the mean drag coefficient lies in the range of $1.0 < C_D(0) < 1.64$ for bare cable and $2.78 < C_D(0) < 3.91$ for cable with 50% area perforated shrouds, respectively.

CONCLUSIONS

Hydrodynamic forces on bare nylon cable and cable with PET shrouds have been studied by self-excitation experiments in steady uniform flows. The main conclusions of this study are summarized as follows.

1. Synchronization for both transverse and in-line cable oscillations occurs in the reduced velocity range of $5.6 < V_r < 8.2$, where the Strouhal number lies in the range of $0.178 < St < 0.159$. Large transverse forces can be induced by cable strumming with the maximum force coefficient of 3.9 occurs near $V_r = 6.6$.
2. The use of moored nylon cables with non-perforated shrouds made from commercial 1.25-liter PET bottles as fish/kelp aggregation devices is probably not practical due to the large hydrodynamic forces induced by vortex shedding. However when the shrouds have a 50% perforated area, both in-line and transverse forces can be reduced considerably.
3. Considerable work remains to determine the best shroud configuration (i.e., diameter, percentage of perforated area and length) suitable for field application as fish/kelp aggregation devices.
4. Perforated shrouds made from commercial PET bottles may also be considered as strumming suppression device for synthetic marine cables.

REFERENCES

1. Every, M. J., R. King and O. M. Griffin, "Hydrodynamic Loads on Flexible Marine Structures Due to Vortex Shedding," *J. of Energy Resources Tech.*, ASME, Vol. 104, 330-336 (1982).
2. Fabula, A. G. and R. L. Bedore, "Tow Basin Tests of Cable Strum Reduction (Second Series)," Naval Undersea Center, NUC TN-1379, San Diego, CA (1974).
3. Goda, Y. and Y. Suzuki, "Estimation of Incident and Reflected Waves in Random Wave Experiments," *Proc. 15th ICCE, ASCE*, 828-845 (1976).
4. Griffin, O. M., "Flow Near Self-excited and Forced Vibrating Circular Cylinders," *J. Engrg. for Ind.*, ASME, Vol. 94, 539-548 (1972).
5. Griffin, O. M. and J. K. Vandiver, "Vortex Induced Strumming Vibrations of Marine Cables with Attached Masses," *Proc. 3rd OMAE*, Vol. 1, 300-309 (1984).
6. Hafen, B. E., D. J. Meggitt and F. C. Liu, "Strumming Suppression-an Annotated Bibliography," Civil Engineering Lab., Technical Report N-1456, Port Hueneme, CA (1976).
7. Peltzer, R. D., "Vortex Shedding in a Linear Shear Flow from a Vibrating Marine Cable with Attached Bluff Bodies," *Proc. 2nd OMAE*, 147-155 (1983).
8. Peltzer, R. D. and D. M. Rooney, "Near Wake Properties of a Strumming Marine Cable: an Experimental Study," *Proc. 3rd OMAE*, Vol. 1, 310-317 (1984).
9. Vandiver, J. K. and T. Y. Chung, "Hydrodynamic Damping on Flexible Cylinders in Sheared Flow," *J. Waterway, Port, Coast. and Ocean Engrg.*, ASCE, Vol. 115, No. 2, 154-171 (1989).
10. Zdravkovich, M. M., "Review and Classification of Various Aerodynamic and Hydrodynamic Means for Suppressing Vortex Shedding," *J. Wind Engrg. and Indus. Aerodynamics*, Vol. 7, 145-199 (1981).
11. Zdravkovich, M. M., "Modification of Vortex Shedding in the Synchronization Range," *J. Fluid Engrg.*, ASME, Vol. 104, 513-517 (1982).

Age Characters of Albacore, Thunnus alalunga, in the Indian Ocean

Ying-Chou Lee and Chin-Lau Kuo

印度洋長鱈鮪之年齡形質

李英周 . 郭慶老

本報告之目的在於研究印度洋長鱈鮪年齡形質，如鱗片、耳石、脊椎骨與背鱈硬棘，之特性及其輪紋判讀之可行性。結果顯示，鱗片、脊椎骨與背鱈硬棘均適合輪紋判讀。又，魚體左側腹後部份鱗片之上部為適合之測量軸；第 18 - 20 節脊椎骨的背後部份為適合之測量軸。

Age Characters of Albacore, Thunnus alalunga, in the Indian Ocean

Ying-Chou Lee* and Chin-Lau Kuo**

ABSTRACT

The characteristics of scale, otolith, vertebra, and spine, and their suitability for age-reading of albacore, Thunnus alalunga, are discussed. The scale, vertebra, and spine are thought to be suitable for age-reading. The scale from the ventral-posterior portion and upper measurement axis will be considered. The 18 - 20th vertebrae and its measurement axis of the dorsal-posterior side will also be adopted.

* Institute of Oceanography, National Taiwan University, Taipei, Taiwan, Republic of China.

** Department of Fishery Biology, Taiwan Fisheries Research Institute, Keelung, Taiwan, Republic of China.

INTRODUCTION

Albacore, Thunhus alalunga, were distributed throughout the Indian Ocean between latitudes 20° N and 40° S, and mainly between 15° S to 35° S (Shimizu 1979). Albacore were caught by Taiwanese, Japanese, and Korean longliners, by France, Spain, and Ivory coast purse seiners, and by Taiwanese gillnetters. The catch of albacore and all of the species by longliners and gillnetters in 1986 and 1987 were shown in Table 1. In 1986, the total catch was about 51,000 MT, and albacore occupied about 51%. Although the percentage by the longliners was not high (30%), however, almost all of the catch (96%) by the gillnetters were albacore. In 1987, the total catch was about 65,000 MT, and albacore occupied only about 35%, however, albacore caught by the longliners and gillnetters occupied only about 31% and 47%, respectively.

Mimura (1957), Kikawa (1966), Ucyanagi (1969), Koto (1969), Suda (1974), Morita (1977), Nishikama et al. (1985), Shiohama (1985a,b; 1986a,b), Huang et al. (1986), and Lee and Lin (1988) have dealt with (1) larvae distribution; (2) movement and distribution; (3) assessment of the stock resource by production model; and (4) determination of the best shape parameter coefficient m and significant age group k , etc., but there were almost none studying the age and growth of albacore in the Indian Ocean. Therefore, the characteristics of scale, otolith, vertebra, and spine were described in this paper, and their possibility for age-reading will be studied.

Relationship between fork length and body weight

The relationship between fork length (FL, cm) and body weight (W, kg) was shown in Fig. 6. Although the samples were composed of larger fish (≥ 70 cm, by longliners) and smaller fish (< 70 cm, by gillnetters), its relationship can be expressed with an

exponential equation: $W = a \cdot FL^b$, and the equations are as follows:

$$\text{Male : } W = 3.383 \times 10^{-5} \cdot FL^{2.8676}$$

$$\text{Female : } W = 4.183 \times 10^{-5} \cdot FL^{2.8222}$$

Characteristics of scale, otolith, vertebra, and spine

Scale, otolith, vertebra, and spine were shown in place 1. The scale was small and thin, however, the rings can be read clearly under the microscope. The percentage of the regenerated scales from six portions of body was shown in Table 2. The occurrence of the regenerated scales in portion A and D were high to 100%, and portion F was the lowest, 30.77%. Fig. 7 shows the mean, standard error (SE), and coefficient of variation (CV) of three measurement axes of portion F. The A measurement axis shows the smallest value of SE and CV, whereas, it is as long as B or C measurement axis. Therefore, the scale was considered to be a good age character, and suitable for age-reading, moreover, portion F and A measurement axis will be adopted in the future studies.

The otolith was oval-shaped, thin, and tiny. It was also fragile and broken easily. Under the microscope, the rings were difficult to identify, therefore the otolith was not considered to be a suitable age character in age determination.

Nine specimens with fork length ranging from 70.7 cm to 71.7 cm were randomly sampled and studied to compare the variation of length, width, and height between 37 vertebrae (Fig. 8). The 1-8th and 30-37th vertebrae appeared a great deal of variation, however, the 9-29th vertebrae appeared rather homogeneous in their length, width, and height. Moreover, the CV values of the 1-8th and 30-37th vertebrae were also greater than those of the 9-29th vertebrae. Fig. 9 shows the growth rate of each vertebra

MATERIALS AND METHOD

Albacore specimens were collected at Kaohsiung fish market from the landings of Taiwanese longliners and gillnetters which operated in the Indian Ocean from December 1985 to April 1988. The fishing areas of the longliners concentrated in three regions: (1) 10° N - 5° S, 85° E - 95° E; (2) central Indian Ocean; and (3) 35° S - 40° S, whereas the gillnetters concentrated in two regions: (1) Arabian Sea and (2) central Indian Ocean (Fig. 1)

After measuring the fork length, body weight, and identification of sex of specimens, the scales were removed from six portions of the left side of the fish (Fig. 2), and the other hard tissues, i.e., otolith, vertebra, and spine were also removed. The percentage of the regenerated scale for each portion was calculated. Three measurements for each scale were also made to determine the most suitable measurement axis of the scale (Fig. 3). The otolith of both sides and the first spine of the first dorsal fin were removed and cleaned with water. The vertebrae were removed and boiled in tap water for about 30 minutes and brushed away remaining connective tissue, and soaked in 3% KOH solution for about 12 hours. After drying, the length, width, and height of each vertebra were measured (Fig. 4), and then were cut by electrical saw horizontally. Four measurements were made for each vertebra to determine the most suitable measurement axis of the vertebra (Fig. 4).

RESULTS

Length frequency distribution

Length frequency distribution of sample specimens from the Taiwanese longliners and gillnetters were shown in Fig. 5. The fish caught by longliners were larger, ranging from 60 cm to 122 cm, mode at 112 - 114 cm, and mean value at 98 cm, however, the fish caught by gillnetters were smaller, ranging from 42 cm to 102 cm, mode at 74 - 76 cm, and mean value at 79 cm.

for fish of 90.5 cm/71.2 cm, 81.3 cm/71.2 cm, and 64.5 cm/71.2 cm. The three curves were separate each other, and their variation were also little, especially for the 9-29th vertebrae, therefore the 9-29th vertebrae were all suitable for age-reading. Also, the CV values at the 18-20th vertebrae were the lowest (Fig. 8). When used for age-reading, 18-20th vertebrae will be adopted. From Table 3, it is also clear that the CV value of the B (dorsal-posterior) measurement axis is the lowest. Therefore, this measurement axis will be used when the vertebra is read and measured.

The first spine of the first dorsal fin was hard. There were no rings can be identified from the outer surface. The spine will be cut by slow-speed saw before reading as Gonzalez-Garces and Farina-Perez (1983), who thought the rings can be read easily and clearly when cutting about 15 mm from the base of the spine. Therefore, the spine seemed to be a suitable age character.

CONCLUSION

The above results show that (1) the scale may be a good age character, but it is difficult to maintain long time; (2) the otolith may be not good, because of its thin, tiny, and fragile characteristics; (3) the vertebra may be a good one, because it is easy for preliminary treatment, and can be maintained long time, however, the vertebra must be sampled from the whole fish body; and (4) the spine also may be a good one, according to Gonzalez-Garces and Farina-Perez (1983).

In the future, we will sample the specimens of albacore from the catch of Taiwanese longliners and gillnetters which operated in the Indian Ocean continuously, and to proceed the age-reading by suitable age characters so as to age and study the growth of the fish.

ACKNOWLEDGMENT

We would like to thank Mr. C.L. Wu and C.S. Huang for their assistance in collecting samples and all of the staff at the Tuna Research Center, Institute of Oceanography, National Taiwan University and Taiwan Fisheries Research Institute, for their assistance with this work.

LITERATURE CITED

- Gonzalez-Garces, A. and A. C. Farina-Perez. 1983. Determining age of young albacore, Thunnus alalunga, using dorsal spines. U.S. Dep. Commer., NOAA Tech. Rep. XMF5, 8:117-122.
- Huang, F. F., C. H. Wang, and H. C. Liu. 1986. Estimation of overall fishing intensity and stock assessment of Indian Ocean albacore (Thunnus alalunga), 1963-1984. FAO/IPTP/TWS/86/34, 23 p.
- Kikawa, S. and M. G. Ferraro. 1966. Maturation and spawning of tunas in the Indian Ocean. Proc. Indo-Pacific Fish. Coun., 12 (11).
- Koto, T. 1969. Studies on the albacore - XIV. Distribution and movement of the albacore in the Indian and the Atlantic Ocean based on the catch statistics of Japanese tuna longline fishery. Bull. Far Seas Fish. Res. Lab., 1: 115-129.
- Lee, Y. C. and H. C. Liu. 1988. An investigation of selecting undermined parameters in fitting the generalized stock production model. Acta Oceanographica Taiwanica, No. 20. (in press).
- Mimura, K. 1957. Studies on the albacore - IV. Fishing condition in the Indian Ocean, especially the size composition in the eastern Seas of the Ocean. Rep. Nankai Reg. Fish. Res. Lab., 5:138-144.
- Morita, S. 1977. On the relationship between the albacore stocks of the south Atlantic and Indian Oceans. ICCAT/SCRS/77/85, 232-237.
- Nishikama, Y., M. Honma, S. Ueyanagi, and S. Kikawa. 1985. Average distribution of larvae of oceanic species of scombroid fishes, 1956-1981. Far Seas Fish. Res. Lab., S. Series 12.

- Shimizu. 1979. State of selected stock of tuna and billfish in the Pacific and Indian Oceans. FAO Fish. Tech. Pap., 200:66-67.
- Shiohama, T. 1985a. Overall fishing intensity and length composition of albacore caught by longline fishery in the Indian Ocean, 1952-1982. FAO/IPTP/TWS/85/22, 91-110.
- Shiohama, T. 1985b. Stock assessment of Indian albacore by production model analysis, 1952-1982. FAO/IPTP/TWS/85/23, 111-118.
- Shiohama, T. 1986a. Overall fishing intensity of longline fishery on albacore in the Indian Ocean, 1952-1984. FAO/IPTP/TWS/86/24, 21p.
- Shiohama, T. 1986b. Stock assessment of Indian albacore by production model analysis, 1952-1984. FAO/IPTP/TWS/86/25.
- Suda, A. 1974. Recent status of resources of tuna exploited by longline fishery in the Indian Ocean. Bull. Far Seas Fish. Res. Lab., 10:27-62.
- Ueyanagi, S. 1969. Observations on the distribution of tuna larvae in the Indo-Pacific Ocean with emphasis on the delincation of the the spawning areas of albacore, Thunnus alalunga. Bull. Far Seas Fish. Res. Lab., 10:27-62.

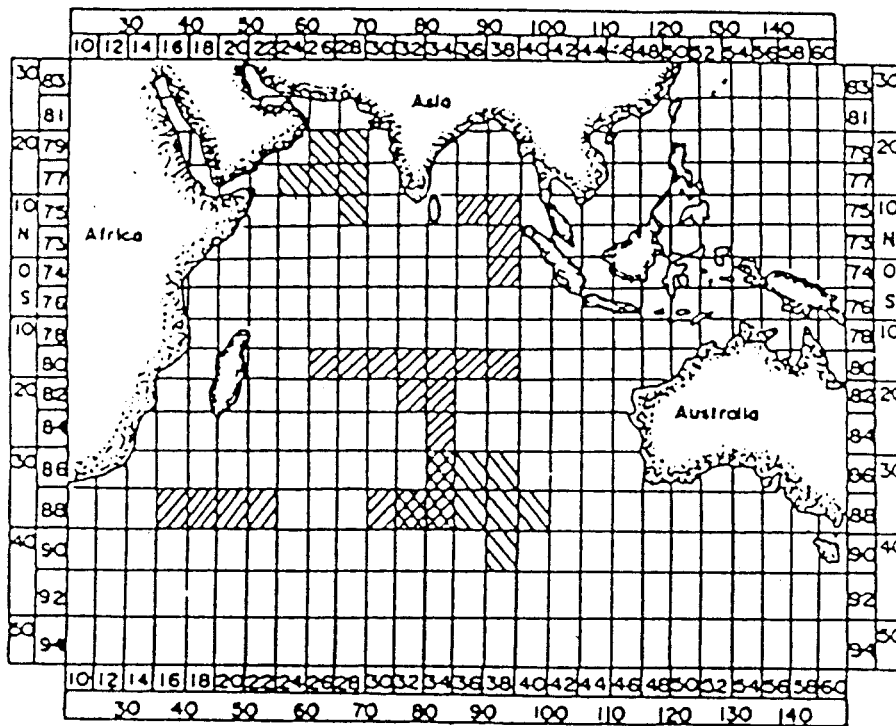





Fig. 1 Sampling area of albacores caught by Taiwanese longliners and gillnetters, December 1985 - April 1988.

-  Fishing area of longliner
-  Fishing area of gillnetter
-  Fishing area of longliner and gillnetter

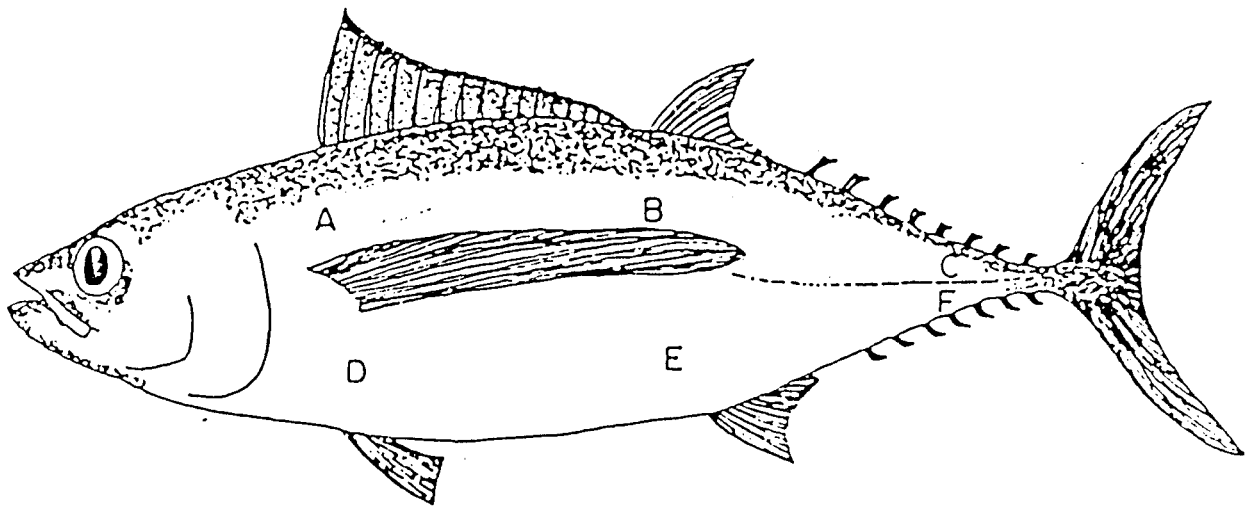


Fig. 2 Sampling portions of scales from albacore.

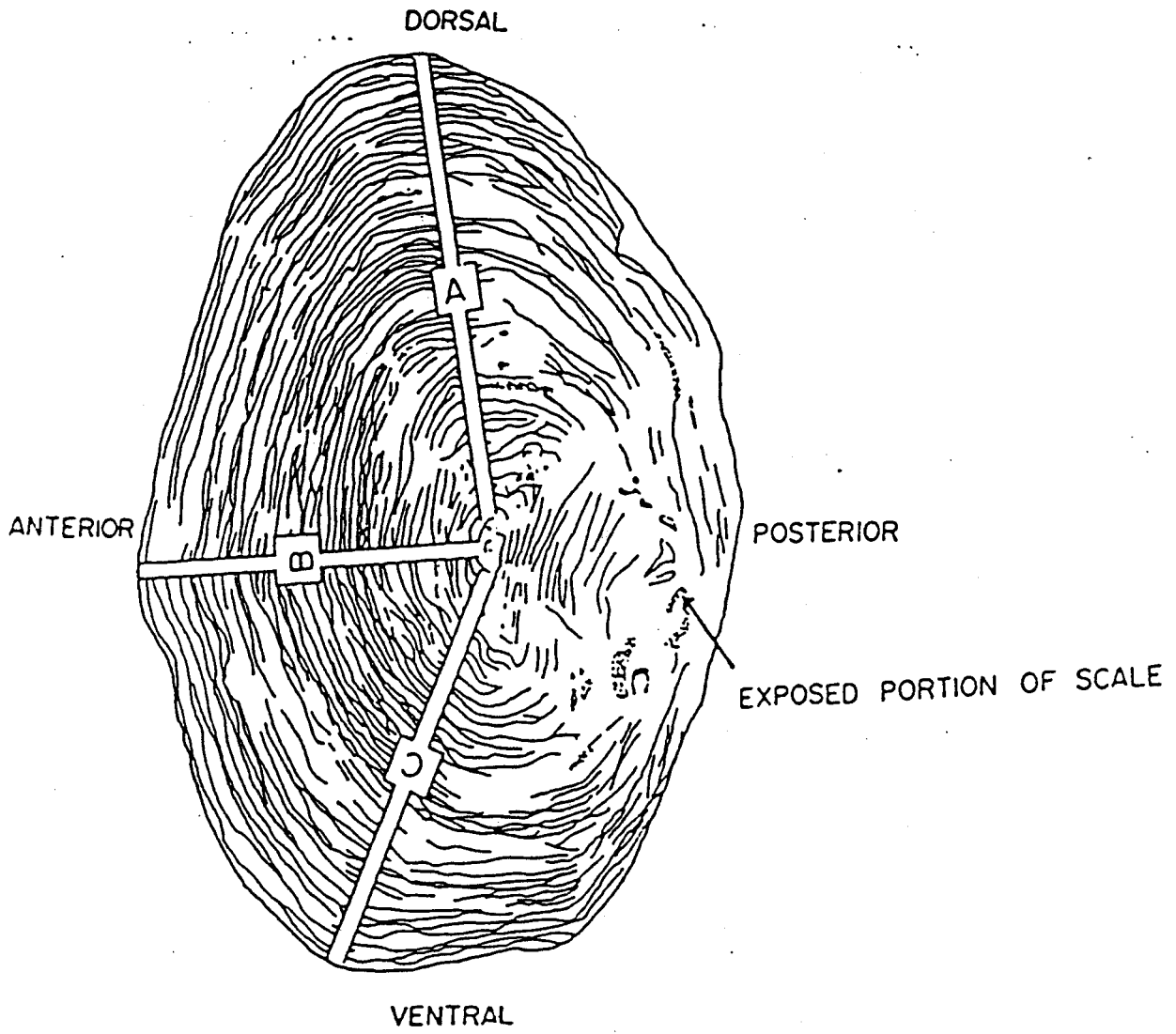


fig. 3 Measurement axis of the scale.

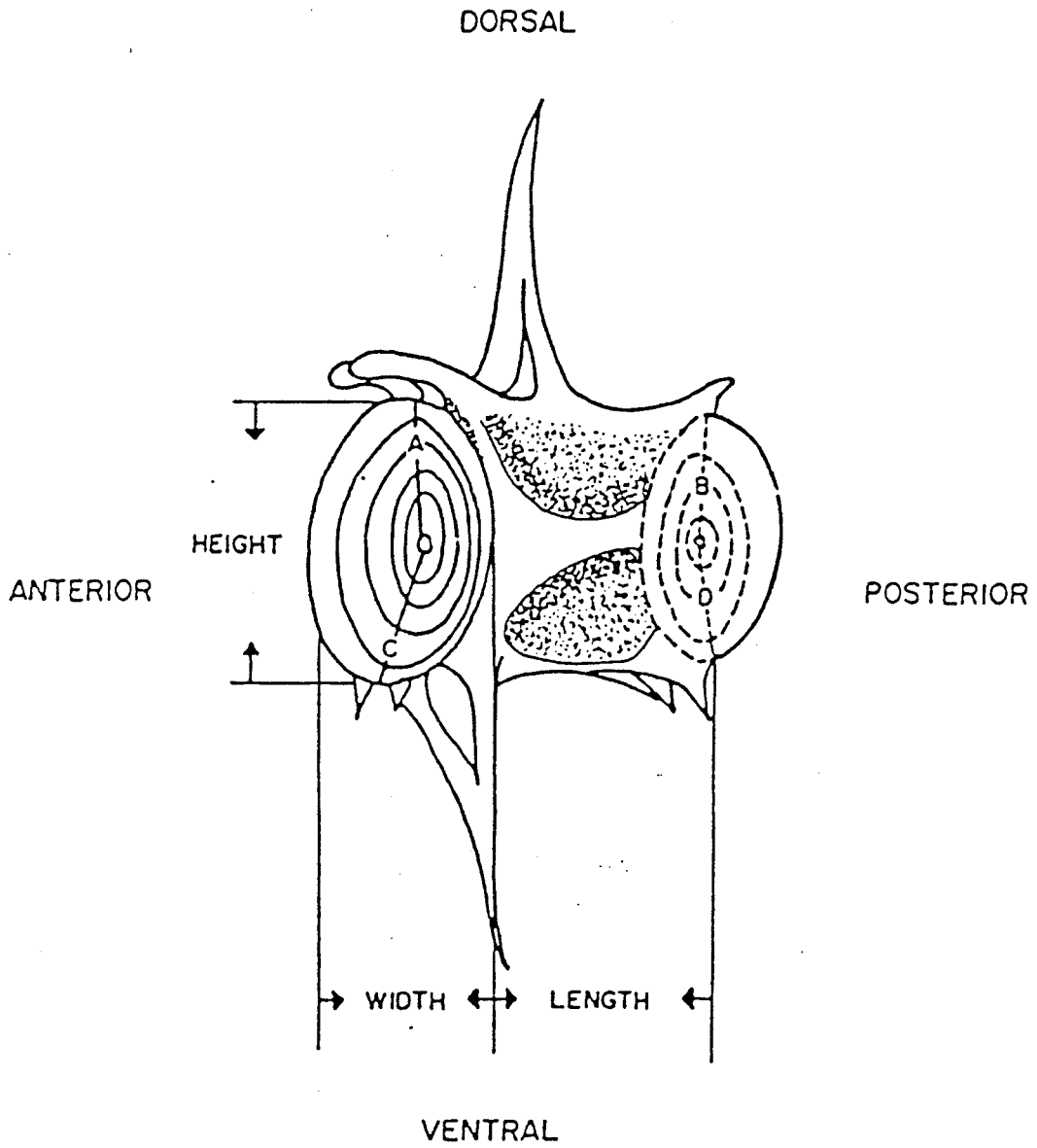


Fig. 4 Length, width, height and measurement axis of the vertebra.

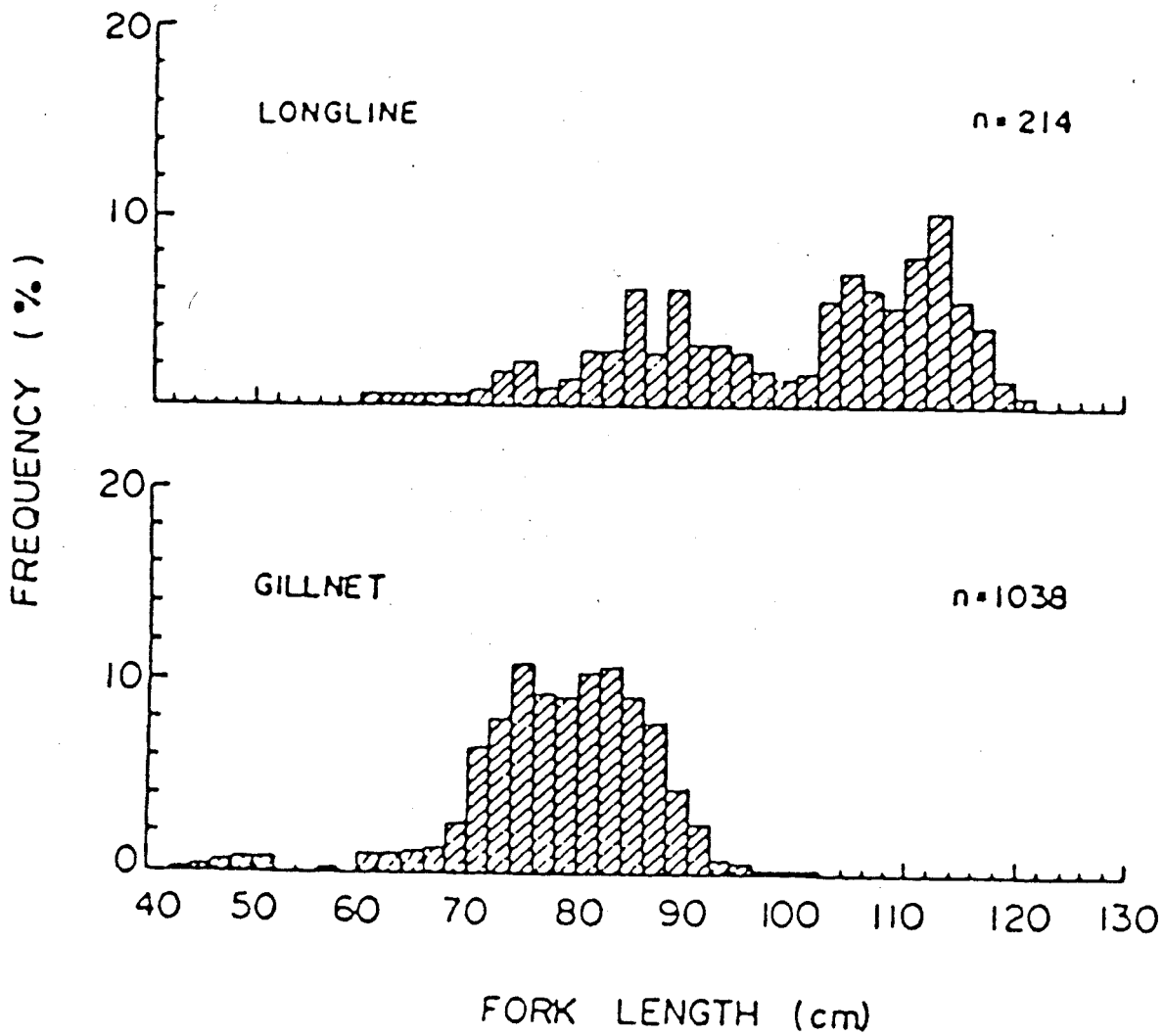


Fig. 5 Length frequency distribution of albacore caught by Taiwanese longliners and gillnetters in Indian Ocean.

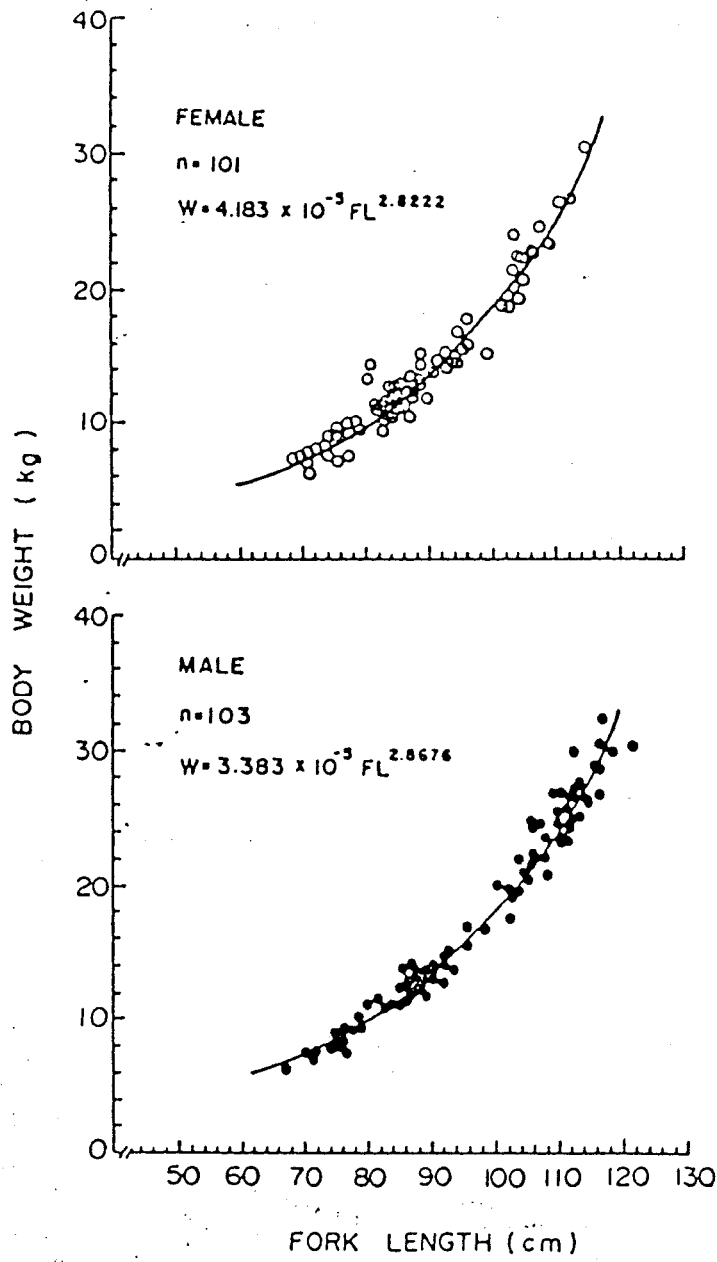


Fig. 6 Relationship between body weight (W) and fork length (FL) of albacore caught from Indian Ocean.

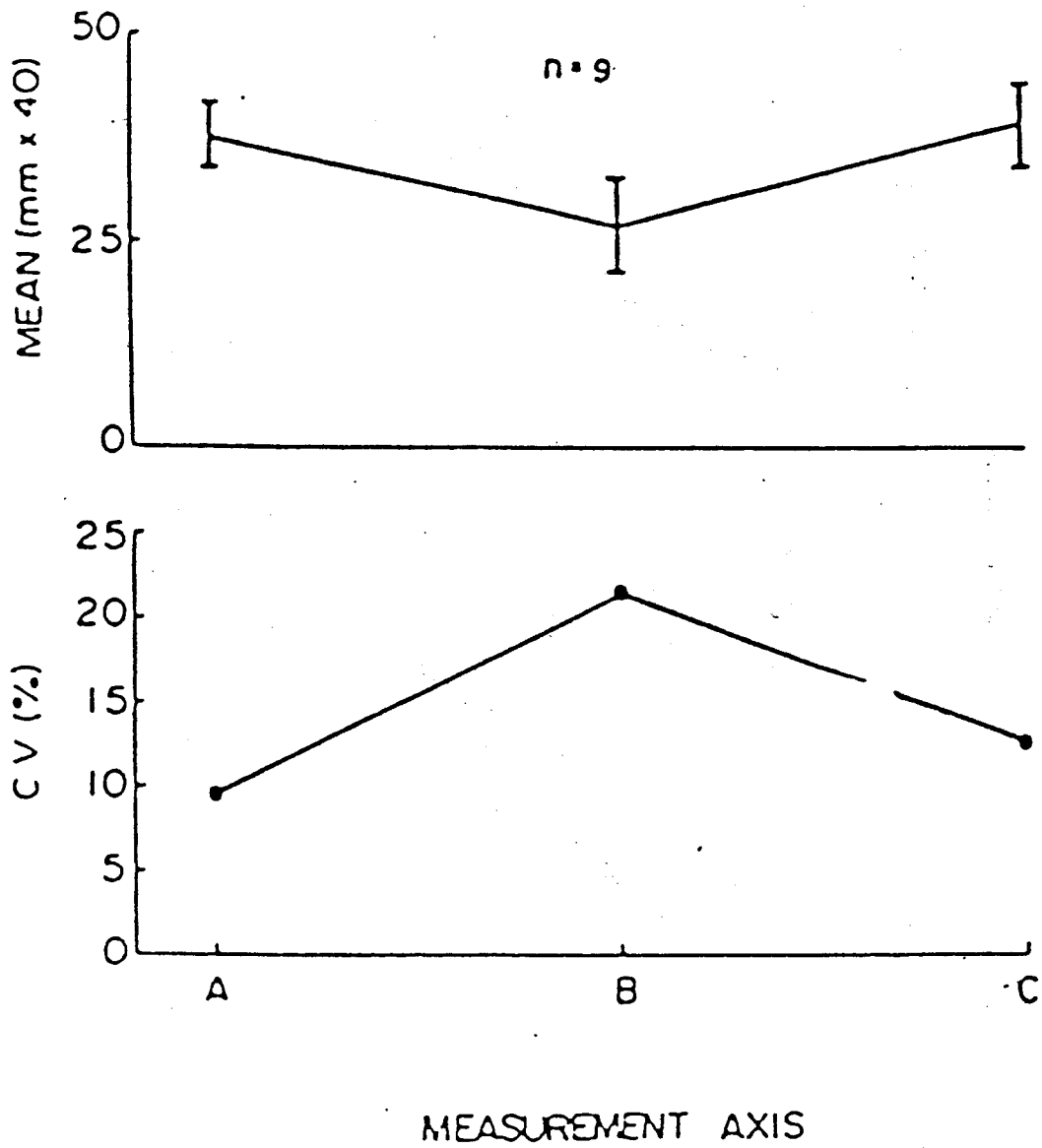


Fig. 7 Mean, standard error (SE) and coefficient of variation (CV) for three measurement axes of the portion F of albacore scales.

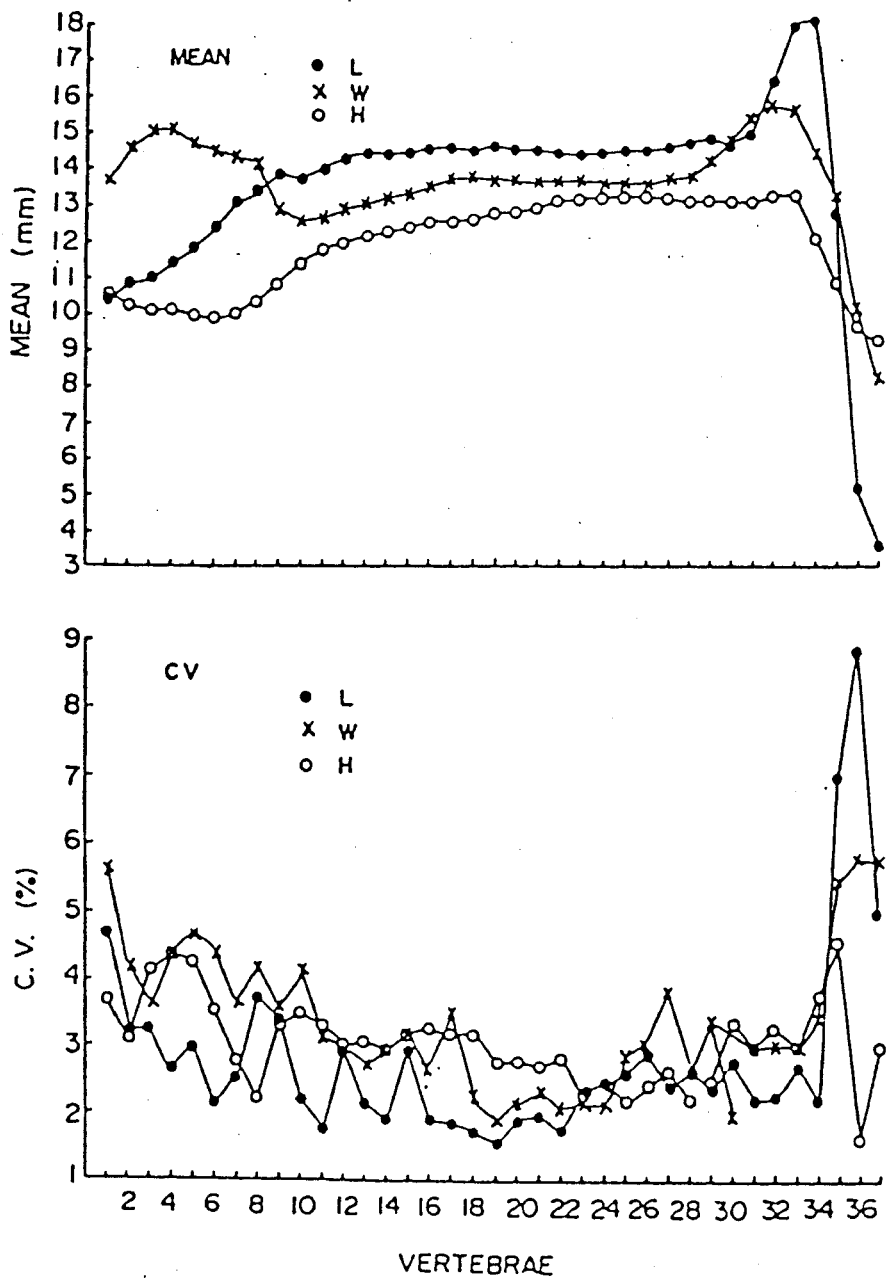


Fig. 8 Curves of means and coefficient of variation (CV) of vertebral length (L), centrum width (W) and centrum height (H) in the sequence of vertebrae. Sample size: 9, fork length: 70.7cm to 71.7cm.

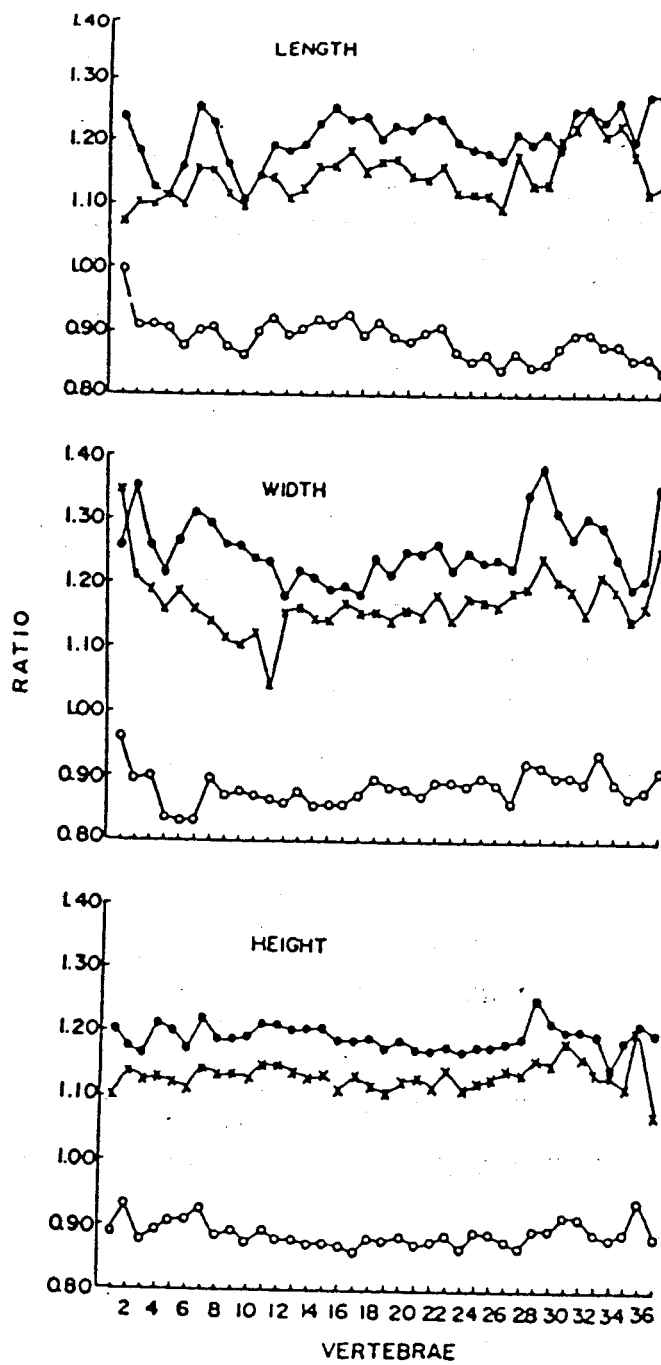


Fig. 9 Growth rates of vertebral length, centrum width and centrum height in the sequence of vertebrae.

• : 90.5cm / 71.2cm, x : 81.3cm / 71.2cm

○ : 64.5cm / 71.2cm.

Table 1. The catch of all species and albacore by the Taiwanese longliners and gillnetters in the Indian Ocean, 1986-1987.

Unit : M.T.

Year	Species	Longliner	Gillnetter	Total
1986	All species	35,143	15,892	51,035
	Albacore	10,708 (30.47)	15,262 (96.04)	25,970 (50.89)
1987	All species	46,504	18,281	64,785
	Albacore	14,203 (30.54)	8,651 (47.32)	22,854 (35.28)

where: the figures in the parenthesis indicate the percentage of albacore.

Table 2. Percentage of regenerative scale from six portions of albacore.

Portion	A	B	C	D	E	F
Regenerative scale	104	106	67	113	233	40
Total specimen	104	133	108	113	262	130
Percentage of regenerative scale (%)	100.00	79.70	62.04	100.00	88.93	30.77

Table 3. Mean, standard error (S.E.) and coefficient of variation (C.V.) of different measurement axes of vertebra.

Unit : μm ($\times 16\times$)

Portion	Statistics	Dorsal-anterior (A)	Dorsal-posterior (B)	Ventral-anterior (C)	Ventral-posterior (D)
18	Mean	64.41	69.56	62.60	67.28
	S.E.	1.85	1.90	3.06	3.22
	C.V. (%)	2.87	2.73	4.89	4.79
19	Mean	65.01	69.73	63.32	68.44
	S.E.	2.73	2.35	3.02	3.71
	C.V. (%)	4.20	3.37	4.77	5.42
20	Mean	66.09	70.91	61.68	67.43
	S.E.	2.92	2.45	3.52	3.38
	C.V. (%)	4.42	3.46	5.71	5.01